AGN and galaxy evolution from deep X-ray surveys

P. Tozzi[1], R. Gilli[2], and the CDFS Team

[1] INAF – Osservatorio Astronomico di Trieste, via G.B. Tiepolo 11, I–34131 Trieste, Italy
  e-mail: `tozzi@ts.astro.it`
[2] INAF – Osservatorio Astronomico di Bologna, via Ranzani 1, I–40127, Bologna, Italy
  e-mail: `roberto.gilli@bo.astro.it`

Abstract. Deep X–ray surveys are providing crucial information on the evolution of AGN and galaxies. We review some of the latest results based on the X–ray spectral analysis of the sources detected in the Chandra Deep Field South, namely: i) constraints on obscured accretion; ii) constraints on the missing fraction of the X–ray background; iii) the redshift distribution of Compton–thick sources and TypeII QSO; iv) the detection of star formation activity in high–z galaxies through stacking techniques; v) the detection of large scale structure in the AGN distribution and its effect on nuclear activity. Such observational findings are consistent with a scenario where nuclear activity and star formation processes develop together in an anti–hierarchical fashion.

Key words. X-rays: diffuse background – surveys – cosmology: observations – X–rays: galaxies – galaxies: active

1. Introduction

In the last years deep X–ray surveys with the *Chandra* and *XMM–Newton* satellites (Brandt et al. 2001; Rosati et al. 2002; Alexander et al. 2003; Hasinger et al. 2001), paralleled by multiwavelength campaigns (see, e.g., GOODS, Giavalisco et al. 2004), provided several crucial information on the evolution of the AGN and galaxy populations. The bold result from the two deepest X–ray fields, the Chandra Deep Field North (CDFN, observed for 2 Ms) and the Chandra Deep Field South (CDFS, observed for about 1Ms) is constituted by the resolution of the X–ray background (XRB) into single sources, mostly AGN, at a level between 80% and 90% (see Bauer et al. 2004 and the recently revised estimate by Hickox & Markevitch 2005), providing an almost complete census of the accretion history of matter onto supermassive black holes through the cosmic epochs. However, the most interesting outcomes go well beyond the demographic characterization of the extragalactic X–ray sky. Indeed, the physical and evolutionary properties of the AGN population are now revealing how they formed and how they are linked to their host galaxies. For the first time, the luminosity function of AGN has been measured up to high redshift. A striking feature is the *downsizing*, or *anti–hierarchical* behaviour, of the nuclear activity: the space density of the brightest Seyfert I and QSO is peaking at $z \geq 2$,

while the less luminous Seyfert II and I peak at $z \leq 1$ (Ueda et al. 2003; Hasinger et al. 2005; La Franca et al. 2005). An analogous behaviour is presently observed in the cosmic star formation history: at low redshift star formation is mostly observed in small objects (see, e.g., Kauffmann et al. 2004), while at redshift 2 or higher, star formation activity is observed also in massive galaxies (with $M_* \sim 10^{11} M_\odot$, see, Daddi et al. 2004a).

The global picture, as outlined by the present data, requires a tight link between the formation of the massive spheroids and the central black holes, as witnessed by the relation between black hole and stellar masses or between black hole mass and the velocity dispersion of the bulge (Kormendy & Richstone 1995; Magorrian et al. 1998; Ferrarese & Merritt 2000). The anti–hierarchical behaviour in both star formation and AGN activity (which reflects in an anti–hierarchical supermassive black holes growth, see Merloni 2004; Marconi et al. 2004; for an alternative view see Hopkins et al. 2005), is envisaged by theoretical models where energy feedback is invoked to self–regulate both processes (see Fabian 1999; Granato et al. 2004).

In these Proceedings, we will describe a few observational results obtained from the latest analysis of the X–ray and optical data in the Chandra Deep Field South and North and which, in our view, are consistent with this picture. In detail, these results concern the following issues:

– the physical properties of AGN from the X–ray spectral analysis of faint X–ray sources;
– the missing fraction of the XRB;
– the distribution of obscured QSO and Compton–thick sources and their relation with the cosmic mass accretion history;
– star formation in high–z galaxies measured in the X–ray band thanks to stacking techniques;
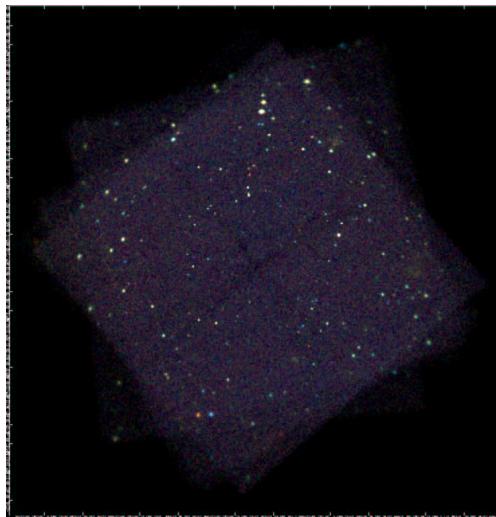– the effects of large scale structure onto nuclear activity.

Fig. 1. The color image of the CDFS (1 Ms exposure, Rosati et al. 2002). The X–ray color code is: red: 0.3–1 keV; green: 1–2 keV; blue: 2–7 keV. Note that fainter sources appear more absorbed (bluer) than brighter ones.

2. Properties of faint AGN from X–ray spectral analysis

The resolution of the XRB, the long–awaited result since its discovery in 1962, has been obtained simply by counting the point sources found in the deep X–ray images taken with the *Chandra* and *XMM–Newton* satellites. This result is clearly shown by the sharp images of the CDFS and the CDFN in Figure 1 and 2. These images also show visually the solution of the so–called *spectral paradox*: fainter sources are more absorbed (and appear bluer in X–ray colors) than brighter ones, so that the total spectrum of the XRB, resulting from the summed contribution of the whole AGN population, has a slope $\Gamma \simeq 1.4$, flatter than that typical of the intrinsic nuclear emission $\Gamma = 1.8$ (as observed in unabsorbed AGN). The resolved fraction of the XRB has been recently revised slightly downwards to be about 80% in both bands (Hickox & Markevitch 2005). AGN makes the 83% and the 95% of the resolved fractions in the soft and in the hard band respectively. On the other hand, star forming galaxies contributes only 3% and 2% (Bauer et al. 2004).
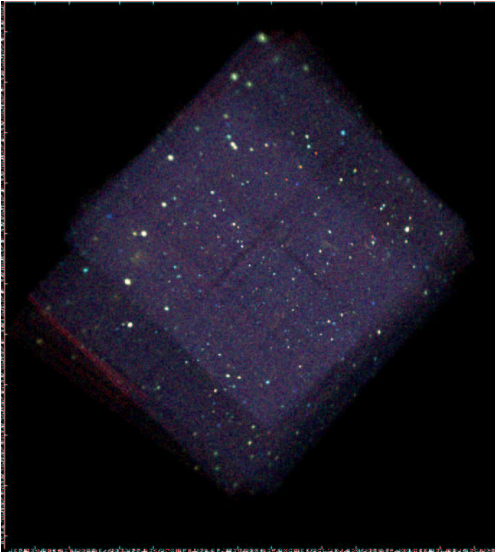
Fig. 2. The color image of the CDFN (2 Ms exposure). Same color code as of Figure 1.

Fig. 3. Intrinsic N_H distribution representative of the whole AGN population in the CDFS. Errors are obtained from the poissonian uncertainties on the number of detected sources in each bin. The dashed curve is a lognormal distribution with $\langle log(N_H)\rangle = 23.1$ and $\sigma = 1.1$. All Compton–thick candidates have been placed in the bin at $N_H = 10^{24}$ cm^{-2} (Tozzi et al. 2006).

However, quoting the resolved fraction of the XRB in the 2–8 keV band is somewhat misleading. Indeed, it has been pointed out that the resolved fraction is significantly decreasing with increasing energy (Worsley et al. 2005). In particular, above 5 keV, the resolved fraction can be as low as 50%. This finding opens again the issue of the resolution of the XRB, requiring the presence of a still undetected population of strongly absorbed AGN at moderate redshift, as can be inferred from the spectral shape of the missing XRB (see Worsley et al. 2005).

The issue of the missing XRB opens several questions on the physical properties of the X–ray sources and calls for a detailed X–ray spectral analysis of the faint AGN population. In a recent Paper (Tozzi et al. 2006) we went through a detailed X–ray spectral analysis of the large majority of the X–ray sources found in the CDFS (321 in the 1Ms catalog after excluding stars and low luminosity sources with $L_X < 10^{41}$ erg s^{-1}, see Giacconi et al. 2002). In particular, the knowledge of the spectroscopic or photometric redshift for almost all the X–ray sources (Szokoly et al. 2004; Zheng et al. 2004), allowed us to measure the value of the intrinsic absorption in terms of equivalent hydrogen column density N_H.
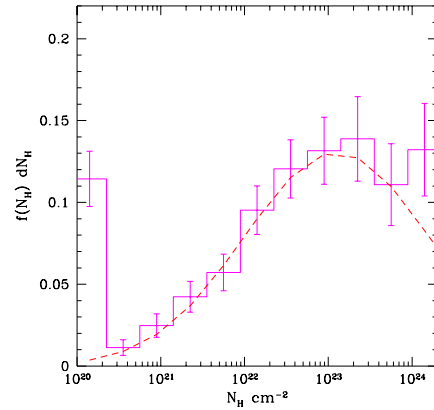
Summarizing the main results of our analysis, we found that the intrinsic spectral slope Γ is always close to the average value $\Gamma = 1.8$, without showing any significant dependence on redshift, intrisic luminosity, or intrinsic absorption. We find significant evidence of the 6.4 keV Fe line in 12% of the sources with spectroscopic redshift. We detect the presence of a soft component (possibly due to partial covering or to scattered emission) in only 8 sources. We measured the intrinsic column density N_H for each source, after freezing the spectral slope $\Gamma = 1.8$ for the faintest ones. The intrinsic N_H distribution has been obtained after correcting for the detection probability as a function of the flux (the sky–coverage) and for sources below the limiting flux of the survey. We find that most of the AGN have high intrinsic absorption with $N_H > 10^{22}$ cm^{-2} (see Figure 3). A fraction of the AGN (more than 10%) are Compton–thick sources, defined as sources with $N_H \geq 1.5 \times 10^{24}$ cm^{-2}. Only few

of these elusive sources are actually detected (we identify only 14 Compton–thick candidates in the CDFS), buth their actual number density is expected to be high. Indeed, due to their spectral shape, well represented by a very hard reflection spectrum, only a small part of their population can be detected by *Chandra*, which is mostly sensitive in the soft band. We also find that about 80% of the sources (among the 139 AGN for which good optical spectra are available), follow a one–to–one correspondence between optical Type I (Type II) and X–ray unabsorbed (X–ray absorbed, defined as sources with $N_H \geq 10^{22}$ cm^{-2}) sources, as predicted by the original version of the unification model for AGN (Antonucci 1993).

3. The missing fraction of the XRB

The detailed knowledge of the spectral shape allows us to better evaluate the detection probability of each source class. This is an important aspect, since the probability of being included in a survey depends significantly on the spectral shape. Therefore, by a careful spectral analysis, we are able to estimate with high accuracy the contribution of the most elusive absorbed sources to the XRB. Indeed, the detection probability is lower for more absorbed sources, since the maximum detectability is achieved in the soft band; therefore, the contribution to the XRB of strongly absorbed sources found in the CDFS is higher than that of sources with the same energy flux but with no or little absorption. This aspect was not fully appreciated in previous works, where the detection probability was only a function of the flux and not of the spectral shape, with a consequent underestimate of the actual number density of the most absorbed sources.

We recompute the resolved XRB in the CDFS, and compare it to the total extragalactic XRB spectrum modeled as a power law with Γ = 1.41 and 1 keV normalization of 11.6 keV cm^{-2} s^{-1} sr^{-1} keV^{-1} (De Luca & Molendi 2004). The contribution to the XRB from CDFS sources is obtained directly by summing the contributed flux from each source weighted by the inverse of the detection probability. The contributed flux in a given energy
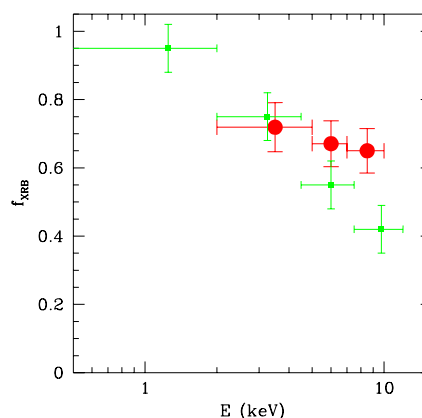

Fig. 4. Red circles: contribution to the resolved XRB in the CDFS in different energy bands. Small green squares are from Worsley et al. (2005).

band is obtained by fitting the X–ray spectrum of each source with a power law plus an intrinsic absorption. We find that the decrease of the resolved fraction as a function of the energy range is not as pronounced as in Worsley et al. (2005), as shown in Figure 4 (Tozzi et al., in preparation). This implies that we are actually seeing a fraction of the population responsible for the missing XRB. Due to the strong absorption, most of these sources can not be detected even in the deepest *Chandra* or *XMM–Newton* surveys, and their discovery must wait for an higher energy, high–sensitivity X–ray mission, or make use of radio or submillimetric data (see Martìnez–Sansigre et al. 2005).

4. AGN and Galaxy formation: TypeII QSO and Compton–thick sources

Another interesting piece of information comes from the redshift distribution of the Compton–thick candidates in the CDFS. As shown in Figure 5, these sources are distributed in a wide range of redshift, a significant part of them around $z \sim 1$. Their redshift and their level of absorption match well with the values expected for the sources responsible of the

missing XRB (see Worsley et al. 2005), reinforcing the reliability of our candidate sources.

Another interesting class of sources are the so called Type II QSO. Since we do not have an optical spectral classification for all the sources, we consider here absorbed QSO, simply defined on the basis of the X–ray properties as bright sources ($L > 10^{44}$ erg s^{-1}) with $N_H > 10^{22}$ cm^{-2}. Some of them have been shown to correspond to Type II QSO on the basis of optical and submm data (Norman et al. 2002, Mainieri et al. 2005a). Most of them are among the optically faint sources of the sample (Mainieri et al. 2005b). We select 54 sources with these properties distributed on a wide range of redshifts (see Figure 6), corresponding to 80% of the sources with $L > 10^{44}$ erg s^{-1} in our sample. We remark that we explore here a limited luminosity range ($L < 10^{45}$ erg s^{-1}), given the small volume sampled. This confirms anyway that Type II QSO constitute a significant fraction of the AGN population.

These findings can be interpreted in the framework of the anti–hierarchical scenario, as described in the Introduction. Absorbed QSO may be sources associated to massive spheroids experiencing at the same time rapid growth of the central black hole and strong star formation activity. In this case, the absorption is not ascribed to circumnuclear matter, as in the simplest version of the unification model, but to the gas distributed on a much wider region strongly polluted by star formation processes. Indeed, the redshift distribution of the QSO population, and therefore of the absorbed ones which represent a significant fraction of it, peaks at a redshift ≥ 2, an epoch when the number density of massive and powerful starburst galaxies is expected to be interestingly high, as found recently with near–IR observations (Daddi et al. 2004, see §5).

The strong energetic feedback from both nuclear activity and star formation in such large objects, is expected to inhibit further accretion and star formation events. On the other hand, smaller objects, where the feedback is less efficient, are able to retain gas that can be accreted subsequently, allowing for episodes of obscured accretion and star formation at lower redshifts.
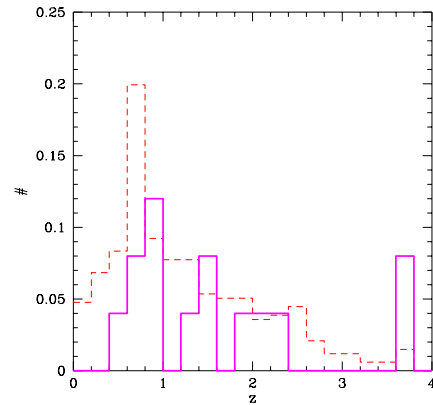

Fig. 5. Normalized redshift distribution of the Compton–thick candidates in the CDFS (14 sources, solid histogram) compared with the normalized distribution of the whole sample (321 sources, dashed histogram).

5. Star formation seen in X-ray at high–z

X–ray emission witnessing star formation events is due to X–ray binaries and hot gas associated with superwinds and SNa remnants. The main advantage of X–ray studies of the cosmic star formation rate is to avoid problems of obscuration, which severely affects optical observations. The price to pay is that, since star forming galaxies have luminosities in the range 10^{39}–10^{42} erg s^{-1}, it is difficult to detect them at high redshifts even in the deepest X–ray surveys. The first normal star–forming galaxy X–ray luminosity function has been derived by Norman et al. (2004) in the combined Chandra Deep Field North and South. The results show an increasing cosmic star formation rate proportional to $(1 + z)^{2.7}$, consistent with other star formation determination in different wavebands. However, the galaxy XLF is determined only at $z \leq 1$, still below the expected maximum of the cosmic star formation history.

On the other hand, other selection techniques, like the one using the B–z vs z–K color diagram (see Daddi et al. 2004b), are able to identify actively star forming galaxies
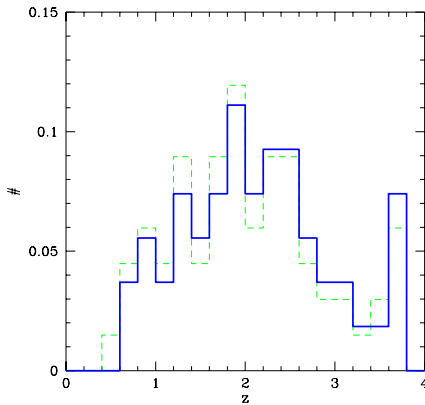
Fig. 6. Normalized redshift distribution of the absorbed QSO in the CDFS (54 sources, solid histogram) compared with the normalized distribution of all the sources with intrinsic X–ray luminosity $L > 10^{44}$ erg s^{-1} (67 sources, dashed histogram)
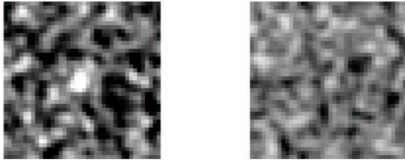

Fig. 7. Stacked X–ray images in the soft (left) and hard (right) band of 22 BzK selected galaxies in the CDFS field (see Daddi et al. 2004b).

at $z \geq 1.4$, with typical stellar masses larger than $10^{11} M_\odot$ and average star formation rate of $\simeq 200 M_\odot$ yr^{-1}. The estimated number density of these $z \sim 2$ star forming galaxies suggests that we are peering into the formation epoch of massive early–type galaxies (Daddi et al. 2004a).

The expected X–ray emission from each one of these high–z, starburst galaxies is below the flux limits of the deepest X–ray surveys. However, we can add together the images of the X–ray fields in the positions of the galaxies, to obtain a stacked image of all the optically selected star forming galaxies. We created the stacked images of 22 *BzK* selected galaxies in the CDFS in the soft and the hard bands. This can be considered an image of about 20 effective Ms of a typical $z \sim 2$ massive, star forming galaxy. The images are shown in Figure 7. In the soft band we detect a total 96 ± 23 net counts, which, for an average spectral slope of $\Gamma = 2.1$, corresponds to an average 2–10 keV rest frame luminosity of 9×10^{41} erg s^{-1}, impliying a star formation rate of about $\sim 190 M_\odot$ yr^{-1} (see Ranalli et al. 2003), in good agreement with the estimate from the reddening–corrected UV luminosities. On the other hand, we have no detection in the observed–frame hard band, confirming the steep spectral slope (hardness ratio $HR < -0.5$ at the 2σ level) and therefore the non–AGN nature of these sources (Daddi et al. 2004b).

This findings confirm that stacking techniques on sources selected in other wavebands, are extremely useful in exploring the level of X–ray emission from star formation at high–z, an aspect which constitutes one of the most compelling scientific cases for the next generation X–ray facilities.

6. Large Scale Structure in deep X–ray surveys

With the spectroscopic follow–up of X–ray sources detected in the CDFS, significant large scale structure has been discovered both in CDFS and CDFN, as shown in Figure 8. In particular, two prominent spikes have been found in the CDFS at $z = 0.67$ and $z = 0.73$ with 19 sources each (Gilli et al. 2003), corresponding to spikes found in the distribution of galaxies in the K20 survey (an ESO–VLT optical and near–infrared survey down to $K \leq 20$ covering part of the CDFS, see Cimatti et al. 2002). Comparing the X–ray and optical catalogs, we found that in the structure at $z = 0.73$, the fraction of active galaxies is the same as in the field, while in the one at $z = 0.67$ it is higher by a factor of 2. We also note that the structure at $z = 0.73$ includes a cluster of galaxies, which may have biased downwards the estimate of the AGN fraction. This finding constitutes one of the first tantalizing hints (significant only at
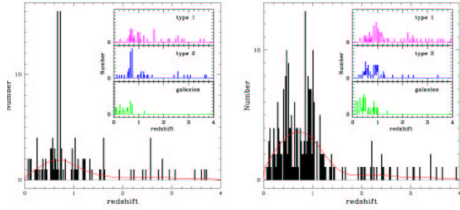
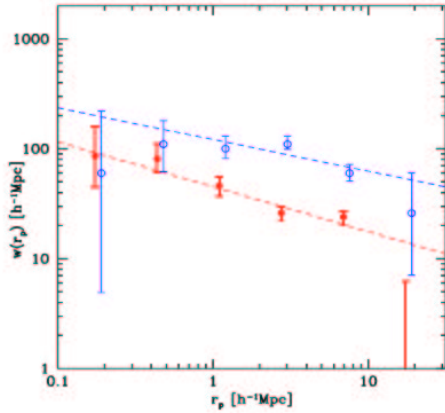**Fig. 8.** Redshift distribution of X–ray sources in CDFS (left) and CDFN (right, Gilli et al. 2005).

Fig. 9. Projected correlation functions of X–ray sources in the CDFS (open circles) and CDFN (filled circles, Gilli et al. 2005).

the 2σ level) that large scale structure can trigger nuclear activity.

Investigation of the spatial clustering of X–ray sources in both fields (Gilli et al. 2005) points out a significant difference in the correlation lengths. We find $r_0 = 8.6 \pm 1.2\,h^{-1}$ Mpc in the CDFS, and $r_0 = 4.2 \pm 0.4\,h^{-1}$ Mpc in the CDFN, with similarly flat slope ($\gamma = 1.33 \pm 0.11$ and 1.42 ± 0.07 respectively), as shown in Figure 9. If we consider only AGN, we obtain higher correlation lenghts, in the range $5 - 10\,h^{-1}$ Mpc. Since at $z \sim 1$ late–type galaxies have a correlation lenght of $\sim 3.2\,h^{-1}$ Mpc while early–type galaxies have $\sim 6.6\,h^{-1}$ Mpc (Coil et al. 2004), the high correlation lengths measured for AGN in the CDFS are consistent with the idea that at $z \sim 1$ AGN with Seyfert–like luminosities are hosted by massive galaxies. The difference in the correlation lengths measured between the two fields dis-
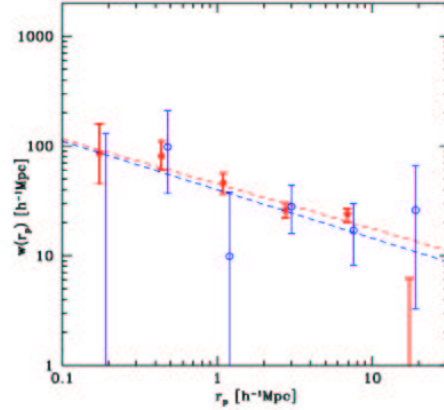

Fig. 10. Spatial correlation functions in the CDFS (open circles) after removal of the two major spikes compared with that measured in the CDFN (filled circles, Gilli et al. 2005).

appears when the two most prominent spikes in the CDFS are removed (see Figure 10). This shows that larger fields of view are needed to kill the cosmic variance and perform a proper investigation of the correlation properties of X–ray detected AGN. We mention two main projects, the COSMOS survey with the *XMM–Newton* satellite (Hasinger et al. in preparation), and the Extended CDFS with *Chandra*. The Extended CDFS complements the original 1Ms exposure with four *Chandra* ACIS-I fields with 250 ks each, bringing the linear size of the field from the former 16 arcmin to 32 arcmin. First results have been published by Lehmer et al. (2005), while spectroscopic follow up is currently under way. The main goal is to better understand the effect of large scale structure onto nuclear activity, and the evolution of the clustering of X–ray sources.

7. Conclusions

We presented few selected topics which we find particularly relevant among the latest results from deep X–ray surveys. We can summarize our conclusions as follows:

- a population of strongly absorbed, possibly Compton–thick AGN at $z \sim 1$ is still missing to the census of the X–ray sky;

the detailed X–ray spectral analysis of faint sources shows that we are detecting some of them, and help us in obtaining a complete reconstruction of the cosmic accretion history onto supermassive black holes;

– we find several absorbed sources (the so–called TypeII QSO) among the population of bright AGN, possibily witnessing the rapid growth of the super massive black holes associated to strong star formation events;

– thanks to stacking techniques, we detected the X–ray emission associated to massive star forming galaxies at redshift as high as $z \sim 2$, therefore peering with X–rays in the epoch of massive galaxy formation;

– investigation of large scale structure in the X–ray detected AGN distribution provides tantalizing hints of its effect on nuclear activity. Studies of spatial correlation of X–ray sources require larger fields of view to kill the cosmic variance and therefore evaluate properly the evolution of the AGN clustering properties.

Such observational findings are providing crucial information on the evolution of AGN and galaxies. Present–day data are consistent with a scenario where nuclear activity and star formation processes develop together in an anti–hierarchical fashion.

References

Alexander, D.M., et al. 2003, AJ, 126, 539
Antonucci, R.R.J. 1993, ARA&A, 31, 473
Bauer, F.E., et al. 2004, AJ, 128, 2048
Brandt, W.N., et al. 2001, AJ, 122, 2810
Cimatti, A. et al. 2002, A&A, 392, 395
Coil, A.L., et al. 2004, ApJ, 609, 525
Daddi, E., et al. 2004a, ApJL, 600, 127
Daddi, E., et al. 2004b, ApJ, 617, 746
De Luca, A., & Molendi, S. 2004, A&A, 419, 837
Fabian, A.C., 1999, MNRAS, 308, L39
Ferrarese, L., & Merritt, D. 2000, ApJL, 539, 9
Giacconi, R. et al. 2002, ApJS, 139, 369
Giavalisco, M. et al. 2004, ApJL, 600, 93
Gilli, R., et al. 2003, ApJ, 592, 721
Gilli, R. et al. 2005, A&A, 430, 811
Granato, G.L., et al. 2004, ApJ, 600, 580
Hasinger, G., et al. 2001, A&A 365, L45
Hasinger, G., et al. 2005, A&A, 441, 417
Hickox, R.C., & Markevitch, M. 2005, ApJ, in press, astro-ph/0512542
Hopkins, P.F., et al. 2005, ApJ, 630, 716
Kauffmann, G., et al. 2004, MNRAS, 353, 713
Kormendy, J., & Richstone, D. 1995, ARA&A, 33, 581
La Franca, F., et al. 2005, ApJ, 635, 864
Lehmer, B. D. , et al. 2005, ApJS, 161, 21
Magorrian, J., et al. 1998, AJ, 115, 2285
Mainieri, V., et al. 2005a, MNRAS, 356, 1571
Mainieri, V., et al. 2005b, A&A, 437, 805
Marconi, A. et al. 2004, MNRAS, 351, 169
Martìnez–Sansigre, A., et al. 2005, Nature, 436, 666
Merloni, A. 2004, MNRAS, 353, 1035
Norman, C., et al. 2002, ApJ, 571, 218
Norman, C., et al. 2004, ApJ, 607, 721
Ranalli, P., Comastri, A., & Setti, G. 2003, A&A, 399, 39
Rosati, P. et al. 2002, ApJ, 566, 667
Szokoly, G. P., et al. 2004, ApJS, 155, 271
Tozzi, P., et al. 2006, A&A, submitted
Ueda, Y., et al. 2003, ApJ, 598, 886
Worsley, M.A., et al. 2005, MNRAS, 357, 1281
Zheng, W., et al. 2004, ApJS, 155, 73